JPE 19-5-22

https://doi.org/10.6113/JPE.2019.19.5.1289
ISSN(Print): 1598-2092 / ISSN(Online): 2093-4718

Optimal Allocation Method of Hybrid Active Power Filters in Active Distribution Networks Based on Differential Evolution Algorithm

Yougen Chen*, Weiwei Chen**, Renli Yang***, and Zhiyong Li†

†,*School of Automation, Central South University, Changsha, China
**China Energy Engineering Group Guangxi Electric Power Design Institute Co., Ltd., Nanning, China
***Maoming Power Supply Bureau, Guangdong Power Grid Co. Ltd., Maoming, China

Abstract

In this paper, an optimal allocation method of a hybrid active power filter in an active distribution network is designed based on the differential evolution algorithm to resolve the harmonic generation problem when a distributed generation system is connected to the grid. A distributed generation system model in the calculation of power flow is established. An improved back/forward sweep algorithm and a decoupling algorithm are proposed for fundamental power flow and harmonic power flow. On this basis, a multi-objective optimization allocation model of the location and capacity of a hybrid filter in an active distribution network is built, and an optimal allocation scheme of the hybrid active power filter based on the differential evolution algorithm is proposed. To verify the effect of the harmonic suppression of the designed scheme, simulation analysis in an IEEE-33 nodes model and an experimental analysis on a test platform of a microgrid are adopted.

Key words: Active distribution network, Hybrid active power filter, Optimal allocation method, Power flow calculation

I. INTRODUCTION

With the increasingly prominent problems of energy depletion and environmental degradation, distributed generation (DG) technology has received more and more attention and application due to its convenience in installation, environmental protection and flexible control. With the vigorous development of DGs, the traditional distribution network is gradually moving to an active distribution network (ADN). The application of an ADN also creates conditions for DG to be incorporated into power networks, which is a trend of the future development of smart distribution networks. The problems of power quality and harmonics generated by grid-connected generation systems have become a bottleneck restricting its development. They also pose great challenges for distribution network planning, grid connection management and operation services [1].

The influence of DG on traditional distribution networks mainly comes from two aspects. First, DGs usually need a converter to connect to the power grid. The actions of power electronic equipment introduce a large number of harmonics into distribution networks. Second, the intermittence and volatility of DG brings serious power quality problems to distribution networks. The uncertainty of DG also causes power quality problems such as voltage fluctuations, voltage flickers and a low power factor [2]. In recent years, the power quality control of DGs, especially harmonic suppression, has been widely studied. In [3], [4], the calculation method of harmonic power flow is studied in order to analyze the harmonic problems in distribution networks. In [5]-[7], control measures for the grid converters of DGs are used to suppress harmonics. The application of passive power filters (PPF) in harmonic control was researched in [8], [9], and active power filters (APF) for harmonic suppression was researched in [10]-[13]. Taking account of the capacity and performance of power filters, hybrid models of an APF and a PPF [14]-[16]

Manuscript received Jan. 11, 2019; accepted Mar. 12, 2019
Recommended for publication by Associate Editor Li Zhang.
†Corresponding Author: lizy@csu.edu.cn
Tel: +86-138-7312-7689, Central South University
*School of Automation, Central South University, China
**China Energy Engineering Group Guangxi Electric Power Design Institute Co., Ltd., China
***Maoming Power Supply Bureau, Guangdong Power Grid Co. Ltd., China

have been rapidly developing. However, this kind of hybrid active power filter (HAPF) has not been studied in the fields of DGs and harmonic control of ADNs.

In order to effectively realize the role of a HAPF in improving power quality, it is important to reasonably allocate the location and capacity of the HAPF to access an ADN. A variety of optimization algorithms have been applied to the optimal allocation of filter devices. In [17], a heuristic algorithm based on a trade-off/risk analysis was proposed, which describes the location and sizing problem of APFs as a multi-objective optimization considering power quality and investment cost. In [18], aiming at the nonlinear problem of APF optimal allocation, an improved harmony search algorithm was designed to obtain the optimal solution for the multi-objective optimization problem. In [19], a cuckoo algorithm was used for the optimal allocation of a power quality regulator in a three-phase unbalance distribution network. In [20], a whale optimization algorithm for the capacity and location of PPFs in radial distribution networks was studies. In [21], an improved particle swarm optimization (PSO) algorithm was proposed to improve the power quality by optimizing the distribution of an APF and shunt capacitor bank. In [22], [23], fuzzy logic was combined with intelligent optimization algorithms such as the imperial competition algorithm and the harmony search algorithm to solve the minimum cost allocation problem of the APFs in distribution networks. In [24], a genetic algorithm (GA) for multi-objective combinatorial optimization of the capacity and position of APFs was studied.

According to the above literature, extensive research on power quality control devices and their optimal allocation has been done. However, there are still some directions lacking in research and methods worth trying in this field. These directions include the following. (1) For the optimal allocation of filters in power grids, current research lacks a suitable scheme for the characteristics of DGs and ADNs. (2) While the APF is mainly used as a filtering device, less research has been done on optimal allocation models for HAPFs. (3) In many intelligent optimization algorithms, the differential evolution algorithm (DEA), as a multi-objective optimization algorithm with convergence and rapidity [25]-[27], has attracted more and more attention in the optimization of power systems. However, it is rarely applied to the optimal allocation of filter devices.

In this paper, a HAPF optimal allocation strategy for an ADN is designed based on a DEA. Taking the ADN as the research object, models of various DG systems in the power flow calculation are established. The improved back/forward sweep algorithm and the decoupling algorithm are used to calculate the fundamental power flow and harmonic power flow, respectively. After that, the optimal allocation model of the HAPF in an ADN is built. Set the initial investment cost of the HAPF as the optimization objective, Then set the aberration rate of the node voltage and the capacity limit of the HAPF as constrained conditions. On this basis, the DEA is applied to multi-objective optimization of the location and capacity of the HAPF. An IEEE-33 nodes distribution system and a microgrid test platform are adopted for simulation and experimental analysis. Results of the simulation and experiment verify the effectiveness of proposed power flow algorithm, as well as the practicability of the optimal allocation scheme of the HAPF in an ADN.

The main contributions of this paper are as follows. (1) According to the output characteristics of different kinds of DGs, their models in power flow calculations are designed. A power flow calculation scheme suitable for an ADN is designed considering the transformation of a DG model with its working conditions. This scheme is suitable for the optimal configuration of a HAPF in an ADN. (2) The influence of the injected PPF and APF on the network parameters is analyzed. The power flow calculation model of the HAPF combines the partial models of PPF and APF. An objective function of the HAPF is designed to minimize the investment cost, which can select the most economical scheme of HAPF allocation while improving power quality. (3) The application of a DEA in the HAPF optimal allocation problem is studied, and the feasibility of the DEA is verified.

This paper is organized as follows. Section II describes mathematical models of a DG and a HAPF in an ADN. Section III designs calculation methods for the fundamental and harmonic power flow. It also mentions the processing methods of different DG nodes. Section IV proposes the optimal model of the HAPF and the differential evolution algorithm used to solve this optimal problem. Section V shows simulation result of the method proposed by this paper. Section VI introduces the experiment platform and an experimental analysis for the proposed method. Section VII provides some conclusion for this paper and further directions for research.

II. Models of DGs and HAPFs in an ADN

A traditional distribution network is a passive power network without DGs, which only receives power from a major power network and has no capacity for self-regulation. Due to the rapid expansion of DG as well as higher and higher requirements in terms of power quality, the ADN has been proposed and developed as a future direction of smart distribution networks [28]. An ADN should satisfy the following two fundamental characters [29], [30].

- An ADN should contain a significant amount of DG, which guarantees its ability to actively regulate and control itself.
- An ADN should transmit electrical power in both directions. That means an ADN can generate power to and receive power from major networks.

Based on the above two principles, the typical structure of an ADN is researched in this paper, which includes the most common types of DG; photovoltaic power generators, wind power generators and micro gas turbines. In this section, models of DGs and HAPFs in an ADN are introduced, which are used for a power flow solution and the optimal allocation of filter devices.

A. Models of Different DGs

There are different forms of DG systems in an ADN, including wind power generation systems (WPGS), photovoltaic power systems (PVPS) and micro gas turbines. All kinds of DG systems produce electric energy in different ways. In addition, there are plenty of modeling methods for DGs based on different targets [31], [32]. In this paper, models of different DGs are mainly used to be added into the power flow calculation by deducting the relationships among the active power, the reactive power and the voltage of DGs. According to their operational characteristics, they can be divided into different types of nodes in the calculation of power flow.

1) Photovoltaic Power Generation Systems: In the calculation of power flow, a PVPS is considered as a PI node, whose output active power and input current are constants, and the injected reactive power Q is as follows:

$$Q=\sqrt{|I|^2\left(e^2+f^2\right)-P^2} \tag{1}$$

in which I is the current injected into the power grid, P is the output active power, and e and f are the real and imaginary parts of the grid voltage. By iterating the grid voltage into Equ. (1), it is possible to obtain the injected reactive power and transform this PI node into a PQ node.

2) Wind Power Generation Systems: The wind generator considered in this paper is an asynchronous wind power generator, which does not have an excitation device itself, and supplies reactive power by the power grid to build a magnetic field. To facilitate the calculation and to simplify the model, the WPGS is treated as a PQ node. When the active power is fixed, the relationship between the voltage and the reactive power of the asynchronous generator is as follows:

$$\begin{cases} U=\sqrt{\dfrac{-P\left(s^2x_\sigma^2+R_e^2\right)}{R_e s}} \\ Q=-\left(\dfrac{U^2}{x_m}+\dfrac{Px_\sigma}{R_e}s\right) \end{cases} \tag{2}$$

where U is the amplitude of the node voltage of the generator, x_σ is the sum of the generator stator reactance and the rotor reactance of the generator, x_m is the excitation reactance, I_R is the rotor current, R_e is the rotor resistance, and s is the slip ratio. In the calculation of the power flow, the output active power P of the WPGS is a constant value. The relationship between the reactive power Q and U can be obtained as:

$$Q=-\frac{U^2}{x_m}+\frac{-U^2+\sqrt{U^2-4P^2x_\sigma}}{2x_\sigma} \tag{3}$$

3) Micro Gas Turbine: A micro gas turbine is a common DG device. It can make an ADN run when it has broken away from the power grid. Its speed control system and excitation system can make it have strong robustness. Therefore, a micro gas turbine can be treated as a PV node.

B. Model of a HAPF

As the main tool for harmonic control, power filters can be divided into PPFs and APFs. A PPF is used to filter low-order harmonics with a higher content. An APF can eliminate high-order harmonics and dynamically track harmonics. The mixed model of a PPF and an APF has been widely developed and applied due to its lower cost and better suppression effect.

1) Partial model of a PPF: For the model of a PPF, let J be the largest number of PPFs that can be installed at node i. The equivalent admittance y_{hij} of each filter's branch under different harmonic orders can be expressed as follows:

$$y_{hij}=\frac{1}{\dfrac{1}{h_{cij}\omega_0C_{ij}q_{ij}}+j\left(\dfrac{h}{h_{cij}^2\omega_0C_{ij}}-\dfrac{1}{h\omega_0C_{ij}}\right)} \tag{4}$$

in which:

$$h_{cij}=\begin{cases} \dfrac{1}{\omega_0\sqrt{L_{ij}C_{ij}}}, & j=1,2,\cdots,J-1, \\ \dfrac{1}{\omega_0R_{ij}C_{ij}}, & j=J, \end{cases} \tag{5}$$

$$q_{ij}=\begin{cases} \dfrac{\sqrt{L_{ij}/C_{ij}}}{R_{ij}}, & j=1,2,\cdots,J-1, \\ \dfrac{L_{ij}}{R_{ij}^2C_{ij}}, & j=J, \end{cases} \tag{6}$$

$$L_{ij}=\begin{cases} \dfrac{1}{h_{cij}^2\omega_0^2C_{ij}}, & j=1,2,\cdots,J-1, \\ \dfrac{q_{ij}}{h_{cij}^2\omega_0^2C_{ij}}, & j=J, \end{cases} \tag{7}$$

$$R_{ij}=\begin{cases} \dfrac{1}{h_{cij}\omega_0C_{ij}q_{ij}}, & j=1,2,\cdots,J-1, \\ \dfrac{1}{h_{cij}\omega_0C_{ij}}, & j=J, \end{cases} \tag{8}$$

h_{cij}, q_{ij}, C_{ij}, L_{ij} and R_{ij} are the resonance number, quality factor, capacitor value, inductance value and resistance value corresponding to the J node filter branch of the i node; $h=1,2,\cdots,H$, $i=1,2,\cdots,N$, $j=1,2,\cdots,J$, H is the maximum order of the harmonic to be filtered, and N is the

number of total network's nodes.

A PPF can filter out harmonics of specific orders in an ADN. This can be regarded as a change of the node admittance matrix when modeling. If a PPF is connected to a node, the node admittance matrix changes to $\boldsymbol{Y^h}+\boldsymbol{\Delta Y}$, which indicates that the admittance matrix is a function of the harmonic order.

$$\boldsymbol{Y^h}=\begin{bmatrix} Y_{11} & \cdots & Y_{1i} & \cdots & Y_{1N} \\ \vdots & & & & \vdots \\ Y_{i1} & \cdots & Y_{ii} & \cdots & Y_{iN} \\ \vdots & & & & \vdots \\ Y_{N1} & \cdots & Y_{Ni} & \cdots & Y_{NN} \end{bmatrix} \tag{9}$$

$$\boldsymbol{\Delta Y}=\begin{bmatrix} \sum_{j=1}^{J} y_{h1j} & 0 & \cdots & 0 \\ 0 & \sum_{j=1}^{J} y_{h2j} & \cdots & 0 \\ \vdots & \vdots & \ddots & \vdots \\ 0 & 0 & \cdots & \sum_{j=1}^{J} y_{hNj} \end{bmatrix} \tag{10}$$

2) Partial Model of an APF: For the model of an APF, let $\boldsymbol{I_{Ah}}$ be the vector of the *h*-order harmonic current I_{Ahi} filtered by all of the APFs in an ADN. In addition, let $\boldsymbol{I_h}$ be the harmonic current vector produced by harmonic sources, and let a_{hi} be the filter coefficient. $\boldsymbol{I_{Ah}}$ can be described as:

$$\boldsymbol{I_{Ah}}=\boldsymbol{A_h}\boldsymbol{I_h},\ h=2,3,\cdots,H,$$
$$\boldsymbol{I_{Ah}}=\begin{bmatrix} I_{Ah1} \\ \vdots \\ I_{Ahi} \\ \vdots \\ I_{AhN} \end{bmatrix},\ \boldsymbol{A_h}=\begin{bmatrix} a_{h1} & & & & \\ & \ddots & & & \\ & & a_{hi} & & \\ & & & \ddots & \\ & & & & a_{hN} \end{bmatrix},\ \boldsymbol{I_h}=\begin{bmatrix} I_{h1} \\ \vdots \\ I_{hi} \\ \vdots \\ I_{hN} \end{bmatrix}. \tag{11}$$

3) Integral Model of a HAPF: Combined with the above two partial models, the admittance matrix equation of a harmonic network changes due to connecting a HAPF to an ADN. The harmonic admittance matrix changes to $\boldsymbol{Y^h}+\boldsymbol{\Delta Y}$. In addition, the harmonic injection current changes to $\left(\boldsymbol{E}-\boldsymbol{A_h}\right)\boldsymbol{I_h}$. Therefore, the harmonic voltage obtained by the admittance matrix equation of a harmonic network is as follows:

$$\boldsymbol{U_h}=\left(\boldsymbol{Y^h}+\boldsymbol{\Delta Y}\right)^{-1}\left(\boldsymbol{E}-\boldsymbol{A_h}\right)\boldsymbol{I_h} \tag{12}$$

III. Calculation of Power Flow in an ADN

In an ADN, calculation of the power flow can be divided into two parts: calculation of the fundamental power flow and calculation of the harmonic power flow. For calculation of fundamental power flow, this section introduces the corresponding processing methods of different DGs. An improved back/forward sweep algorithm is used to calculate the fundamental power flow. For the calculation of the harmonic power flow, a decoupling algorithm is designed for this purpose.

A. Calculation Method of the Fundamental Power Flow

There are several mature methods of power flow solution such as the Newton-Laphson method and the PQ decoupled method, which have great applications in the power flow calculation of transmission networks. However, the differences between distribution networks and transmission networks make the computer algorithms mentioned above less efficient. Considering simplicity, astringency and amount of calculation, the back/forward sweep algorithm is an appropriate method to solve power flow of distribution networks.

Because of various DGs, a large number of PQ, PV and PI nodes need to be processed in calculation of the power flow for an ADN. Furthermore, in the calculation, the different working states of DGs may need different processing methods. The improved back/forward sweep algorithm is used due to its good performance in dealing with all kinds of DG nodes.

1) Processing Methods of Different DG Nodes: For PQ nodes, if the DG simultaneously produces both active and reactive power, the injection active power P_L and reactive power Q_L of the load node where the DG is located is changed to:

$$P_L+jQ_L=-P-jQ+P_l+jQ_l \tag{13}$$

where P and Q are the active power and reactive power produced by the DG, and P_l and Q_l are the active power and reactive power in the load node. If the DG only produces active power, and absorbs reactive power from the power grid, the injection power of the load node is changed to:

$$P_L+jQ_L=-P+jQ+P_l+jQ_l \tag{14}$$

The injection current of the DG in the load node is solved by:

$$I=\frac{P-jQ}{U}=\frac{(P-jQ)U}{|U|^2} \tag{15}$$

For PV nodes, because the active power and voltage of the PV node are constant, each node's reactive power is improved by variation of the voltage as follows:

$$\boldsymbol{Q^{k+1}}=\boldsymbol{Q^k}+\boldsymbol{\Delta q^k} \tag{16}$$

$$\boldsymbol{J\Delta q^k}=\boldsymbol{\Delta U^k} \tag{17}$$

where $\boldsymbol{\Delta q^k}$ is the change of the reactive power at the solution time *k*, and $\boldsymbol{\Delta U^k}$ is the difference of the voltage. $\boldsymbol{J}$ is a sensitivity matrix, which is similar to the impedance matrix in

the distribution network. However, its value is negative. The diagonal elements of $\boldsymbol{J}$ are the self-impedances at the DG nodes, and the non-diagonal elements are the mutual impedances.

If the reactive power generated by the DG exceeds its rated value in the above solving process, it is considered that the reactive power of the DG has reached its maximum value. In this case, the PQ node is used to replace the PV node. When the calculation is carried out, if the voltage amplitude is greater than the given value, the PQ node is replaced by the PV node.

For PI nodes, since the output active power and the current of the PI node are constants, its reactive power can be solved by Equ. (1). In addition, a PI node can be transformed to a PQ node.

2) Calculation Process of the Back/forward Sweep Algorithm: To calculate the fundamental power flow, the branches of an ADN are stratified and numbered. The branch currents and the node voltages are constantly updated during the back/forward calculation. If the reactive power of a PV node is out of bounds, this node will turn into a PQ node. The calculating steps are as follows.

Step 1: Initialize the voltages of each node: $U_i(0)=1$, $i=0,\ 1,2,\cdots,n$.

Step 2: Calculate the injection current of each node:

$$I_{Ni}=\frac{S_i}{U_i} \tag{18}$$

where S_i is the injection power of node *i*, U_i is the voltage of node *i*, and $\boldsymbol{I_N}=\left[I_{N1},I_{N2},\cdots,I_{Nn}\right]^T$ is the current vector of the injection currents.

Step 3: Forward calculation: the relationship between branch's current vector $\boldsymbol{I_L}=\left[I_{L1},I_{L2},\cdots,I_{Ln}\right]^T$ and the injection current vector of node $\boldsymbol{I_N}$ is as follows:

$$\boldsymbol{I_N}=\boldsymbol{AI_L} \tag{19}$$

Let $\boldsymbol{A_0}=\boldsymbol{A}+\boldsymbol{E}$, where $\boldsymbol{E}$ is an identity matrix with the same order as $\boldsymbol{A}$. $\boldsymbol{A_0}$ is a matrix whose diagonal elements are zero and the other elements are same as those of $\boldsymbol{A}$. $\boldsymbol{I_L}$ can be obtained by the following formula:

$$\boldsymbol{I_L}=\boldsymbol{A_0I_L}-\boldsymbol{I_N} \tag{20}$$

The current through the branch *i* is:

$$I_{Li}=\sum_{j=i+1}^{n}A_{ij}I_{Lj}-I_{Ni} \tag{21}$$

Step 4: Back calculation: the node voltage U_i can be calculated by:

$$U_i=\sum_{j=1}^{i-1}A_{ij}U_j-Z_{ii}I_{Li} \tag{22}$$

Step 5: Distinguish the conditions of convergence.

B. Calculation Method of the Harmonic Power Flow

Nowadays, harmonic flow algorithms are divided into three main categories. These categories include the linear algorithm, nonlinear algorithm and decoupling algorithm. The decoupling algorithm combines the advantages of linear and nonlinear methods. It reduces the memory and improves the speed of computing and convergence. Because the fundamental power flow is much larger than the harmonic power flow, the function of the harmonic source is ignored when the fundamental power flow is solved. The fundamental power flow is solved first. Then the harmonic power flow is calculated. The concrete steps are as follows.

Step 1: Initialize the voltage of each node.

Step 2: Calculate the fundamental power flow in the ADN, and obtain the fundamental voltage amplitude of all nodes.

Step 3: Suppose the harmonic voltages of each order are zero, and every harmonic current is solved by the relation between the fundamental voltage and the *h*-order harmonic current.

The converter is the most important harmonic sources in an ADN. For the three-phase rectifying device, the fundamental current I_1 and the harmonic current I_h can be expressed as:

$$I_1=\frac{3U}{4\pi X_s}\left(e^{-i2\alpha}-e^{-i2(\alpha+\gamma)}-i2\gamma\right) \tag{23}$$

$$I_h=\frac{\sqrt{3}U}{\pi X_s}\cos\frac{h\pi}{6}\left(\begin{array}{l}\dfrac{1}{h(h+1)}\left(e^{-i(h+1)\alpha}-e^{-i(h+1)(\alpha+\gamma)}\right)\\ -\dfrac{1}{h(h-1)}\left(e^{-i(h-1)\alpha}-e^{-i(h-1)(\alpha+\gamma)}\right)\end{array}\right) \tag{24}$$

where X_s is the equivalent impedance, *h* is the harmonic order, and α is the initial phase angle. γ is the reduplication angle, which can be obtained by:

$$I_d=\frac{\sqrt{6}U}{2X_s}\left(\cos\alpha-\cos(\alpha+\gamma)\right) \tag{25}$$

The ratio of the harmonic current can be calculated by Equ. (26).

$$HRI_h=\frac{2}{h}\sqrt{\begin{array}{l}\left(\dfrac{\sin\frac{h-1}{2}\gamma}{h-1}\right)^2+\left(\dfrac{\sin\frac{h+1}{2}\gamma}{h+1}\right)^2-\\ 2\left(\dfrac{\sin\frac{h-1}{2}\gamma}{h-1}\right)\left(\dfrac{\sin\frac{h+1}{2}\gamma}{h+1}\right)\cos(2\alpha+\gamma)\end{array}}{\sin^2\gamma-2\gamma\sin\gamma\cos(2\alpha+\gamma)+\gamma^2} \tag{26}$$

Step 4: The node equation is used to solve the harmonic voltages of each node until the condition is satisfied. When

the decoupling algorithm is used to calculate the harmonic currents, the network equation of the harmonic admittance matrix is as follows:

$$\boldsymbol{Y}^{h}\boldsymbol{U}^{h}=\boldsymbol{I}^{h} \tag{27}$$

The harmonic voltage of each node can be solved by Equ. (27). Due to the distortion of harmonics, the effective value of the harmonic node voltage is:

$$\left|U_i\right|=\sqrt{\sum_{h=1}^{H}\left|U_i^h\right|^2} \tag{28}$$

Step 5: The total harmonic voltage distortion rate THD_{Ui} on node i is as follows:

$$THD_{Ui}=\frac{\sqrt{\sum_{h=2}^{H}\left|U_i^h\right|^2}}{\left|U_i^h\right|},\quad i=1,2,\cdots,n \tag{29}$$

IV. Optimal Allocation of HAPFs

In this section, the optimal allocation method of a HAPF in an ADN is analyzed. The initial investment cost of the HAPF is taken as the objective function. The voltage distortion of each node and the capacity of the HAPF are used as constrained conditions. The differential evolution algorithm is used to solve the optimal problem.

A. Optimal Allocation Model of HAPFs

1) Optimization Objective: The central idea of this paper is to reduce the investment cost of the filter devices in an ADN. The optimal allocation aims to improve the installation of filters to obtain the minimum cost and the best filtering effect. The objective function is determined as the total investment for the installation of filter devices:

$$\min\left[\sum_{i=1}^{N}\sum_{j=1}^{J}\mu_{ij}f_{Fij}\left(Q_{CNij}\right)+\sum_{i=1}^{N}\nu_i f_{Ai}\left(S_{Ni}\right)\right] \tag{30}$$

where μ_{ij}, ν_i are used to indicate whether PPF parts or APF parts are installed. $\mu_{ij}=1$ means connecting a PPF j at node i. Meanwhile, $\mu_{ij}=0$ means there is no PPF installed in this branch. The meanings of $\nu_i=1$ and $\nu_i=0$ are the same as above. S_{Ni} represents the rated compensation of the APF connected to node i, and Q_{CNij} represents the rated compensation of a PPF j connected to node i. $f_{Ai}\left(S_{Ni}\right)$ defines the relationship between the cost of the APF and its installed capacity, $f_{Fij}\left(Q_{CNij}\right)$ defines the relationship between the cost of the PPF and its installed capacity. $f_{Ai}\left(S_{Ni}\right)$ and $f_{Fij}\left(Q_{CNij}\right)$ are determined by the price coefficient function in the market:

$$f_{Ai}\left(S_{Ni}\right)=b_{0i}+b_{1i}S_{Ni} \tag{31}$$

$$f_{Fij}\left(Q_{CNij}\right)=a_{0ij}+a_{1ij}Q_{CNij} \tag{32}$$

where a_{0ij}, a_{1ij}, b_{0i} and b_{1i} are determined by the price of capacitors, reactors and resistors in the market.

The relationship between the installed capacity of a PPF and its capacitance and inductance can be represented as follows:

$$Q_{CNij}=U_i^2\omega sC_{ij}+\frac{I_h^2}{h\omega sC_{ij}}=U_i^2\omega sL_{ij}+\frac{I_h^2}{h\omega sL_{ij}} \tag{33}$$

where U_i is the fundamental voltage of node i, I_h is the harmonic current of h order, s is the power factor, and ω is the fundamental angle frequency.

2) Constraint Conditions: Constraint conditions are proposed to ensure stable and safe operation at the minimum cost. In addition, the harmonic distortion rate of the whole distribution network's voltage should be below its specified value, which means a stable relationship among the voltage, current and capacity of the network.

- Constraint conditions of the harmonic distortion rate

Let HRU_{hi} be the voltage distortion rate of the h-order harmonic of node i, and $UTHD_i$ be the total voltage harmonic distortion rate of node i, which should satisfy the following inequalities:

$$HRU_{hi}=\frac{U_{hi}}{U_{li}}\times 100\%\le c_{HRU} \tag{34}$$

$$UTHD_i=\frac{\sqrt{\sum_{h=2}^{H}U_{hi}^2}}{U_{1i}}\times 100\%\le c_{UTHD} \tag{35}$$

where U_{hi} is the harmonic voltage of the h order of node i, U_{li} is the fundamental voltage, and c_{HRU} and c_{UTHD} are the maximum values required for the voltage distortion rate of the h-order harmonic and the total voltage distortion rate.

- Constraint conditions of the capacity of a PPF

$$\sqrt{\frac{Q_{C1ij}}{\omega}}+\sum_{h=2}^{H}\sqrt{\frac{Q_{C1ij}}{h\omega}}\le K_U\sqrt{\frac{Q_{C1ij}}{\omega}} \tag{36}$$

$$\sqrt{\omega Q_{C1ij}+\omega\sum_{h=2}^{H}hQ_{Chij}}\le K_I\sqrt{\omega Q_{CNij}} \tag{37}$$

$$Q_{C1ij}+\sum_{h=2}^{H}Q_{Chij}\le K_Q Q_{CNij} \tag{38}$$

Eqns. (36), (37) and (38) are the voltage, current and capacity constraint conditions of the PPF of each branch. Among the above inequalities, Q_{C1ij} and Q_{Chij} are the fundamental and h-order harmonic compensation of the PPF j connected to node i. K_U, K_I and K_Q are the permissible over-voltage, over-current and over-capacitance coefficients of the capacitor in the PPF.

- Constraint conditions of an APF

The capacity of an APF is determined mainly by the compensated harmonic current value, as shown in the

following formula:

$$S_{Ai}=\sqrt{\left(U_{1i}^2+\sum_{h=2}^{H}U_{hi}^2\right)\sum_{h=2}^{H}I_{Ahi}^2} \tag{39}$$

Its constraint condition of the capacity is:

$$S_{Ai}\le K_S S_{Ni} \tag{40}$$

where S_{Ai} is the capacity of the APF, I_{Ahi} is the *h*-order harmonic current of the APF at node *i*, U_{1i} and U_{hi} are the fundamental and *h*-order harmonic voltage of node *i*, K_S is the permissible overcapacity coefficient of the APF, and S_{Ni} is the rated capacity of the APF at node *i*.

B. Optimization Scheme Based on the Differential Evolution Algorithm

The differential evolution algorithm is an intelligent random search algorithm, which has the ability of global search. Using real number coding and variation operation based on the difference, a new individual is produced by a vector difference among individuals in a population. The generation of new individuals in random operations improves the population's gene. At the same time, the difference algorithm also has the ability of memory, which can dynamically track the current search.

Focus on the minimum optimization problem: $\min f(x_1,x_2,L,x_D), s.t.\ L_j\le x_j\le U_j,\ j=1,2,L,D$, where L_j and U_j are the lower and upper limits of the variable x_j, and D is the dimension of the variable space.

Step 1: Initialization. Randomly generate the initial population: $\left\{x_i(0)\middle|L_{ij}\le x_{ij}\le U_{ij}, i=1,2,\cdots,n\right\}$. Generate the variable *j* of the individual *i*:

$$x_{i,j}(0)=L_{i,j}+\text{rand}(0,1)\left(U_{i,j}-L_{i,j}\right) \tag{41}$$

Step 2: Variation operation. The individual variation is completed by the difference method. Three different individuals are randomly selected from the population. The vector difference between two individuals is added to the variant individual.

$$V_{i,j}(t+1)=x_{a_1,j}(t)+F\left(x_{a_2,j}(t)-x_{a_3,j}(t)\right), i\ne a_1\ne a_2\ne a_3 \tag{42}$$

Step 3: Crossover operation. The values of the *t* generation $\{x_i(t)\}$ and its variant temporary individual $P_{i,j}(t+1)$ are determined according to the following conditions. If $\text{rand}(0,1)\le CR$ or $j=j_{rand}$, $P_{i,j}(t+1)=V_{i,j}(t+1)$. If not, $P_{i,j}(t+1)=x_{i,j}(t)$. $CR\in(0,1)$ and $j_{rand}\in[1,D]$.

Step 4: Selection operation. The tournament selection strategy is used to determine which individuals enter the next generation.

$$x_i(t+1)=\begin{cases}P_i(t+1), & \text{fit}\left(P_i(t+1)\right)\le\text{fit}\left(x_i(t)\right)\\ x_i(t), & \text{fit}\left(P_i(t+1)\right)>\text{fit}\left(x_i(t)\right)\end{cases} \tag{43}$$

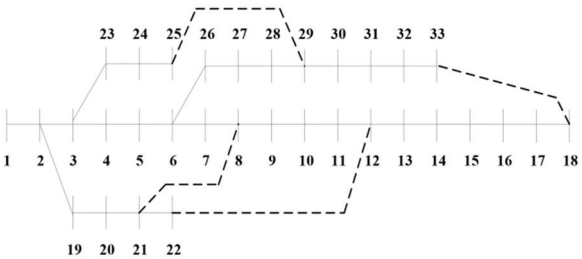

Fig. 1. Wiring diagram of an IEEE-33 nodes distribution system.

Step 5: At last, whether or not the population number is less than the convergent condition is judged. If the condition is not satisfied, let $t=t+1$ and return the variable operation. Otherwise, the iterative calculation is finished.

In the differential evolution algorithm, the following parameters have a great influence on the performance of the algorithm.

(1) Population *n*: The larger the population size, the slower the iteration speed, but the easier it is to find the global optimal solution. In general, $n\in[30,500]$.

(2) Scaling factor *F*: The scaling factor is a variable between 0 and 2. The size of the scaling factor is proportional to the global search capability, and inversely proportional to the convergence speed of the algorithm.

(3) Cross factor *CR*: The cross factor is a variable between 0 and 1. In crossover operation, a bigger cross factor can result in a faster speed for population replacement and a narrower search range.

In practical application, the above parameters need to be continuously adjusted and experimented to obtain the optimal value.

V. Simulation Analysis

An IEEE-33 nodes distribution system is used as a simulation example, and a connection diagram of the system is shown in Fig. 1. For the parameters of this system refer to [21]. The voltage reference is 12.66*kV*, the power reference is 100*MVA*, node #1 is set to the balance node, the voltage of system bus is $1.0\angle 0°$, the voltage amplitude ε_1 of the convergent node and the iterative precision ε_2 of the voltage amplitude of the PV node are all set to 10^{-8}.

A. Calculation Method of the Fundamental Power Flow

In order to verify the feasibility of the algorithm, the access of a DG is divided into five cases.

Case 1 only inserts a DG of the PQ type at node #6.

Case 2 inserts a DG of the PQ type at node #6, and inserts a DG of the PI type at node #15.

Case 3 adds a DG of the PV type at node #20 on the basis of Case 1 and Case 2.

Case 4 inserts multiple DGs of the PQ type to nodes #6, #9 and #10, respectively.

TABLE I
PARAMETERS OF EACH DG

Number of Access Node	Capacity for Access	Type of DG
6, 9, 10	$P=400kW, Q=100kVar$	PQ
15, 16, 17	$P=100kW, I=50A$	PI
20	$P=600kW, V=12.66kV$	PV

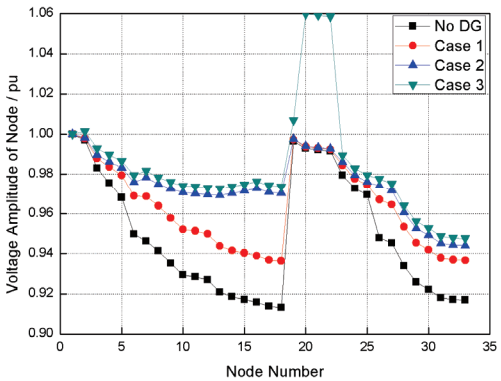

Fig. 2. Voltage amplitudes comparison of one DG inserted into a single node.

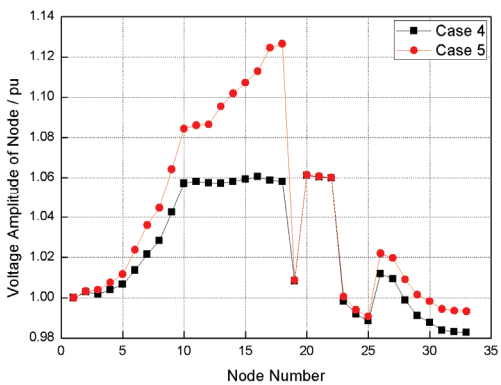

Fig. 3. Voltage amplitudes comparison of DGs of the same type inserted into different nodes.

Case 5 adds multiple DGs of the PI type to nodes #15, #16 and #17 based on Case 3.

The parameters of each DG are shown in Table I.

The voltage amplitudes obtained from the flow calculation of the five cases above are shown in Fig. 2 and Fig. 3. It is known from the figures that the voltage amplitudes of the nodes increase with different DG access. Comparing Case 3 to Case 1 and Case 2, it can be seen that because a DG of the PV type is connected to node #20, the voltage amplitudes of the nearby nodes are increased. For Case 4 and Case 5, with the same DGs inserted to different nodes, most of nodes' voltage amplitudes are over 1.0, and the highest value appears on node #18 of Case 5, which has a voltage amplitude of 1.1265. A large amount of power is injected into the power grid, resulting in an increase in the active power of the power grid. Therefore, the voltage amplitude increases, especially in the vicinity of the DG. The analysis above is fit for the calculation results of the fundamental power flow, which can verify the effectiveness of the proposed calculation method.

TABLE II
PARAMETERS OF THE HARMONIC SOURCE

Parameter	Value
Control Angle α	$\alpha=0$
Constant DC I_d	$I_d=200A$
Equivalent Impedance X_S	$X_S=40\Omega$

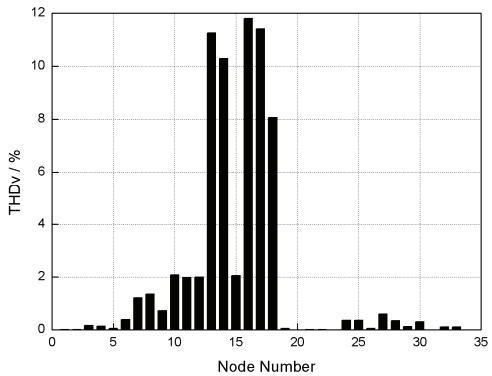

Fig. 4. Voltage distortion rate of each node.

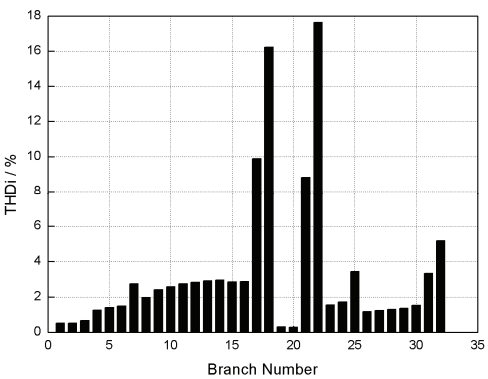

Fig. 5. Current distortion rate of each branch.

B. Calculation Method of the Harmonic Power Flow

A harmonic wave source is added to a distribution network, and the harmonic flow is calculated and analyzed. It is assumed that a six-pulse rectifying load with a large capacity, as shown in Table II, was connected to node #18 and the conditions of other loads and DGs reference Case 3.

The harmonic power flow is solved by the decoupling algorithm, and the total harmonic voltage distortion rate of each node is shown in Fig. 4. The total voltage distortion rate near node #18 reaches the maximum, and the voltage distortion rates of distant nodes are smaller.

Fig. 5 shows the current distortion rate of each branch. All 32 branch currents are distorted. The distortion rates of the voltage and current are bound to have a significant impact on the stable operation of the distribution network. Therefore, it is necessary to filter the power distribution network to achieve the required distortion rate.

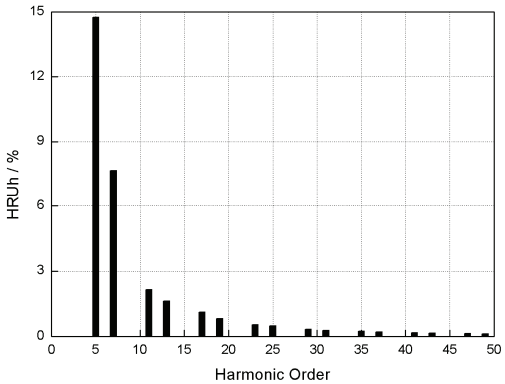

Fig. 6. Harmonic current content of each harmonic current.

TABLE III
PARAMETERS OF THE OPTIMAL MODEL

Parameter	Value	Parameter	Value
c_{HRU}	3.20	K_S	1.00
c_{UTHD}	4.00	a_{0ij}	20
K_U	1.10	a_{1ij}	15
K_I	1.30	b_{0i}	45
K_Q	1.35	b_{1i}	50

TABLE IV
PARAMETERS OF THE DIFFERENTIAL EVOLUTION ALGORITHM

Parameter	Value
Population *I_NP*	100
Number of iterations *I_itermax*	100
Scaling factor *F_weight*	0.85
Cross factor *F_CR*	1

Fig. 6 shows the harmonic current content of each harmonic current. Due to the large rectifying devices of the six thyristors, there are only harmonics of the $6k+1$ orders, $k=1,2,3,\cdots$. The contents of the fifth, seventh, eleventh and thirteenth harmonics are large. The higher the harmonic order is, the smaller the content rate is.

According to the character of the harmonic source, the voltage distortion rates of the node with the harmonic source and its adjacent nodes reach a high level. In addition, the branch current distortion rates connecting these nodes also reach a high level. Furthermore, the frequency of each harmonic in the ADN is related to the characteristics of the harmonic source. The above calculation results of the harmonic power flow have verified this analysis, which means the proposed calculation method can obtain correct results of the harmonic power flow.

C. Results of the Optimal Allocation

1) Parameters of the Model: The parameters of the optimization model are given in Table III. The relevant parameters of the differential evolution algorithm are shown in Table IV.

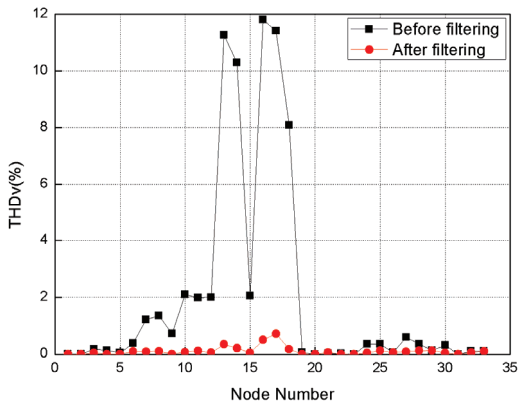

Fig. 7. Optimal allocation for a single harmonic source.

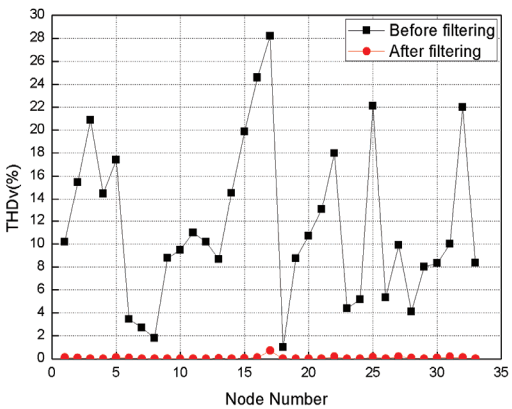

Fig. 8. Optimal allocation for multiple harmonic sources.

2) Optimal Allocation for a Single Harmonic Source: In this case, only a single harmonic source is added to node #18. The optimal allocation results of the HAPF are shown in Table V and Table VI. According to the parameters given in Tables III, V and VI, it can be calculated that the cost of installing such hybrid filters is 0.216 million USD, and the number of iterations of the differential evolution algorithm is 50.

Fig. 7 is a comparison of the power distortion rate of each node after adding the HAPF. After adding the HAPF, the voltage distortion rate of each node clearly drops, and the filtering effect is good.

3) Optimal Allocation for Multiple Harmonic Sources: In an actual distribution network, the network nodes are various and complex with strong randomness. In order to be close to reality, nodes #22, #25, #33 and #3 are connected to the same harmonic devices as node #18. The same differential evolution algorithm is used to optimize the design. The results are shown in Table VII and Table VIII. The total cost reached 0.559 million USD, and the differential evolution algorithm maximum iteration number reached 80.

In the case of multiple harmonic sources, the voltage distortion rate of each node is very serious, as shown in Fig. 8. When multiple groups of HAPFs are installed in the ADN, the distortion rate of the harmonic voltage is obviously

TABLE V
OPTIMIZATION RESULTS OF A PPF WITH A SINGLE HARMONIC SOURCE

Access Node	Time of Resonance	Quality Factor q	C/F	L/H	Q_{CN} / *MVar*
17	7	35	6.3781×10^{-5}	3.2000×10^{-3}	3.06

TABLE VI
OPTIMIZATION RESULTS OF AN APF WITH A SINGLE HARMONIC SOURCE

Access Node	Absorption Coefficient a_{hi}						S_{Ni} / *MVar*
	h=5	h=7	h=11	h=13	h=17	h=19	
16	0.9931	0.9377	0.9510	0.8644	0.8450	0.5461	0.78

TABLE VII
OPTIMIZATION RESULTS OF A PPF WITH MULTIPLE HARMONIC SOURCES

Access Node	Time of Resonance	Quality Factor q	C/F	L/H	Q_{CN} / *MVar*
17	7	35	6.3781×10^{-5}	3.2000×10^{-3}	3.06
5	11	45	1.4099×10^{-5}	5.9452×10^{-3}	0.66
26	5	60	7.8171×10^{-5}	5.1900×10^{-3}	3.71
23	13	45	0.8666×10^{-5}	6.9000×10^{-3}	0.41

TABLE VIII
OPTIMIZATION RESULTS OF AN APF WITH MULTIPLE HARMONIC SOURCES

Access Node	Absorption Coefficient a_{hi}						S_{Ni} / *MVar*
	h=5	h=7	h=11	h=13	h=17	h=19	
16	0.9842	0.9573	0.9451	0.9122	0.7414	0.6452	0.56
32	1.0450	0.9451	0.9198	0.7561	0.7142	0.6418	1.45

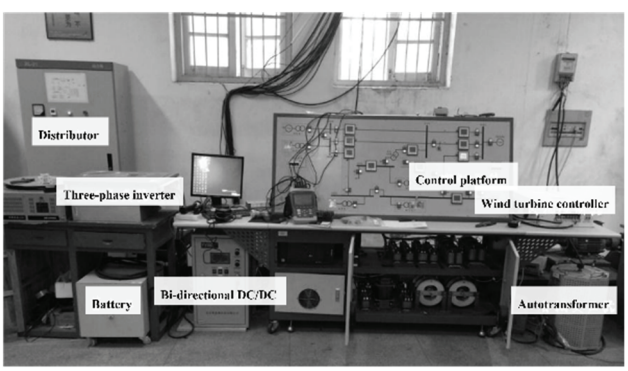

Fig. 9. Location diagram of each subsystem in a physical installation.

weakened, and the power quality is improved. The simulation results verify the feasibility of the optimization algorithm used in this paper.

VI. EXPERIMENTAL ANALYSIS

An experimental platform of a power system and a microgrid is used for experimental analysis. This platform includes a photovoltaic power generation system, wind power generation system, energy storage system and monitoring system. Fig. 9 is a location diagram of each subsystem. Fig. 10 shows the material objects of the photovoltaic array and

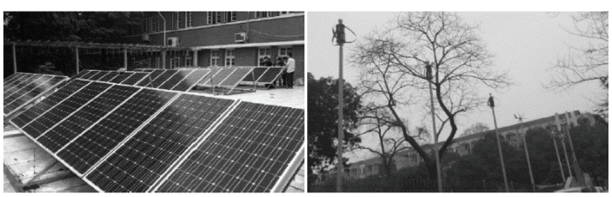

(a) (b)

Fig. 10. Experimental facilities. (a) Photovoltaic array. (b) Wind turbines.

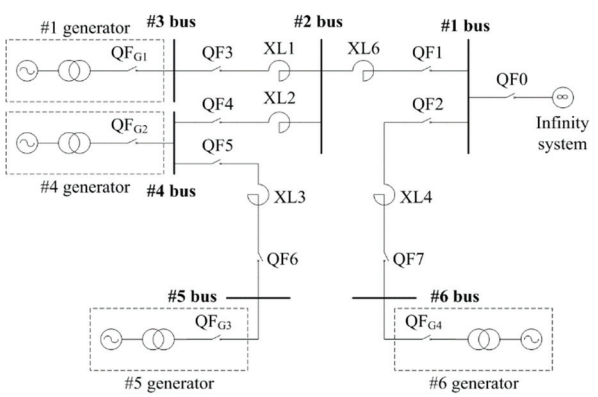

Fig. 11. Main electrical connections of the experimental platform involved in this paper.

micro wind power system. The main electrical connection of the experimental platform involved in this paper is shown in

TABLE IX
MAJOR PARAMETERS OF THE EXPERIMENTAL PLATFORM

Name	Parameter
#1 generator	Synchronous generator, P=4kW, Q=3.6kW
#4 generator	Wind turbine, P=4kW, Q=3.6kW
#5 generator	Photovoltaic system, P=2kW, I=9A
#6 generator	Photovoltaic system, P=10kW, I=15A
XL1, XL2	L=38mH
XL3	L=8mH
XL4	L=26mH
XL6	L=13mH
#1 bus	P=0, Q=0, U=1.0pu
#2 bus	P=0, Q=0, U=0pu
#3 bus	P=4kW, Q=3.6kW, U=0pu
#4 bus	P=4kW, Q=3.6kW, U=0pu
#5 bus	P=4kW, Q=3.6kW, U=0pu
#6 bus	P=4kW, Q=3.6kW, U=0pu

TABLE X
VOLTAGE AMPLITUDE OF EACH LINE

Number of Bus	Voltage of Line A/V	Voltage of Line B/V	Voltage of Line C/V
#1	377.7	380.4	380.6
#2	382.1	384.2	383.5
#3	378.7	381.5	380.8
#4	379.1	382.2	382.8
#5	379.5	382.8	382.9
#6	379.1	382.7	382.6

Fig. 11, and its major parameters are listed in Table IX.

A. Fundamental Power Flow

The results of the measurement on the control platform are compared with the results of the power flow calculation method used earlier. The results displayed on the measuring device are shown in Table X. Notice that the voltage is expressed by the line voltage.

Results of the theoretical calculation are shown in Table XI. Comparing results from Table X with those from Table XI, the measured values and the calculated values are very close. Therefore, the correctness of the theoretical and practical application can be obtained.

B. Harmonic Power Flow

The parameters of the harmonic source and the high-power adjustable resistance box are shown in Table XII.

The voltage distortion rate of each bus is measured in three cases.

Case 1: $I_d = 0.79A$, connected to #3 bus.

Case 2: $I_d = 1.82A$, connected to #3 bus.

Case 3: $I_d = 1.82A$, connected to #2 bus.

TABLE XI
POWER FLOW CALCULATION VALUES FOR THREE PHASE INVERTERS

Number of Bus	Voltage Amplitude of Node/pu	Effective Value of node Voltage/V	Phase Angle
#1	1.0000	380.00	0
#2	1.0000	380.00	0
#3	1.0000	380.00	0
#4	1.0000	380.00	0
#5	1.0000	380.00	0
#6	0.9999	379.96	0

TABLE XII
PARAMETERS OF THE HARMONIC SOURCE AND THE HIGH-POWER ADJUSTABLE RESISTANCE BOX

Name	Parameter
Harmonic Source	Trigger angle $\alpha = 0°$, output DC voltage $U_d = 445V$
High-power adjustable resistance box	Resistance $R = 560\Omega/245\Omega$, current $I = 0.79A/1.82A$

In different cases, the measured values of the voltage distortion of each bus are compared with the calculated values, as shown in Table XIII. It can be seen from Table XIII that when the harmonic source is connected to the network, the voltage distortion rate of each bus increases greatly except for the balance node. The error between the algorithm of this paper and the measured value is small.

In different cases, the measured values of the voltage distortion of each bus are compared with the calculated values, as shown in Table XIII. It can be seen from Table XIII that when the harmonic source is connected to the network, the voltage distortion rate of each bus greatly increases except for the balance node. The error between the algorithm of this paper and the measured value is small.

C. Optimal Allocation for the Experimental Platform

In three cases, the algorithm of this paper is used to optimize the allocation, and the results are shown in Table XIV. The results of the optimal allocation show that only the active power part of the HAPF is needed, and the installation position of the filter is consistent with the access point of the harmonic source.

As shown in Table XIV, only one 25A active power part of the HAPF needs to be installed in the three cases. After connecting the filter, the voltage distortion rate of each bus decreases. The measured values and the calculated values are given in Table XV.

In conclusion, the test platform only needs to install the active power part of the HAPF with a capacity of 25A, which is in the same position as the connecting position of the harmonic source device. The obtained experimental results verify the feasibility and effectiveness of the method in this paper.

TABLE XIII
MEASURED VALUES AND CALCULATED VALUES OF THREE CASES

Number of Bus	Voltage distortion/%					
	Case 1		Case 2		Case 3	
	Measured values	Calculated values	Measured values	Calculated values	Measured values	Calculated values
#3	25.7	23.4	36.1	34.2	19.6	20.5
#4	9.4	10.6	12.4	11.9	19.3	18.9
#5	9.3	9.0	12.4	12.1	19.1	20.4
#6, #1	2.2	4.3	2.0	3.8	2.2	2.5
#2	9.3	8.8	12.5	11.2	19.8	21.4

TABLE XIV
OPTIMIZATION RESULT OF THE APF IN THREE CASES

Case	Access Node	Absorption Coefficient a_{hi}						S_{Ni} / *MVar*	Expense/USD
		h=5	h=7	h=11	h=13	h=17	h=19		
Case 1	1	0.9993	0.9888	0.9041	0.8937	0.6784	0.4397	0.011	45.55
Case 2	1	1.0002	0.9547	0.9258	0.7195	0.5489	0.5512	0.024	46.20
Case 3	7	0.9974	0.9614	0.9361	0.8743	0.7658	0.7130	0.022	46.10

TABLE XV
VOLTAGE DISTORTION RATES OF THE HARMONIC POWER SUPPLY BEFORE AND AFTER THE CONNECTING FILTER

Number of Bus	Voltage distortion/%								
	Case 1			Case 2			Case 3		
	Before	After		Before	After		Before	After	
		Measured values	Calculated values		Measured values	Calculated values		Measured values	Calculated values
#3	23.4	2.1	1.9	34.2	3.9	1.8	20.5	2.8	2.0
#4	10.6	1.9	3.8	11.9	2.0	4.0	18.9	2.9	3.1
#5	9.0	1.8	3.5	12.1	3.1	3.4	20.4	3.4	2.9
#6, #1	4.3	2.3	1.7	3.8	2.3	2.2	2.5	1.2	1.6
#2	8.8	3.6	2.5	11.2	1.6	2.5	21.4	2.5	2.1

VII. CONCLUSION

DGs are incorporated into traditional distribution networks to form ADNs, which affect traditional distribution networks in different degrees. The power quality problem is one of the most common and the most serious problems in the power grid. The aim of this paper is to optimize a HAPF in an ADN with DG systems. The calculation of the fundamental power flow is carried out by the back/forward sweep method, and the harmonic power flow is solved by the decoupling algorithm. The optimal allocation of the HAPF is designed based on the differential evolution algorithm. This algorithm is programmed in the MATLAB environment, and applied to a microgrid test platform. The results of the calculations and measurements verify the feasibility and effectiveness of the proposed optimal allocation scheme. The method discussed in this paper still has some limitations in terms of the application objects. In a follow-up study, different situations will be considered in order to be more practical.

ACKNOWLEDGMENT

The authors would like to thank the support of the Natural Science Foundation of Hunan Province (No. 2015JJ2171) and the Fundamental Research Funds for the Central Universities of Central South University (No. 2018zzts522) for the research in this paper.

REFERENCES

[1] M. Z. Fortes, V. H. Ferreira, I. S. Machado, and W. C. Fernandes, "Harmonic analysis of distributed generation in Smart City Bzios project," *IEEE Workshop on Power Electronics and Power Quality Applications (PEPQA)*, pp. 1-5, 2015.

[2] G. Ding, F. Gao, Y. Tang, L. Zhang, and S. Zhang, "A novel harmonic control approach of distributed generation converters in a weak microgrid," *Applied Power Electronics Conference and Exposition (APEC)*, pp. 2132-2139, 2014.

[3] S. Wang, X. Liu, K. Wang, L. Wu, and Y. Zhang, "Tracing harmonic contributions of multiple distributed generations

in distribution systems with uncertainty," *Electr. Power Energy Syst.*, Vol. 95, pp. 585-591, Feb. 2018.

[4] A. K. Tagore, and A. R. Gupta, "Harmonic load flow analysis of radial distribution system in presence of distributed generation," *International Conference on Power and Embedded Drive Control (ICPEDC)*, pp. 147-151, 2017.

[5] X. Wang, F. Blaabjerg, and Z. Chen, "Autonomous control of inverter-interfaced distributed generation units for harmonic current filtering and resonance damping in an islanded microgrid," *IEEE Trans. Ind. Appl.*, Vol. 50, No. 1, pp. 452-461, Jan./Feb. 2014.

[6] H. Tian, Y. Li, and P. Wang, "Hybrid AC/DC system harmonics control through grid interfacing converters with low switching frequency," *IEEE Trans. Ind. Electron.*, Vol. 65, No. 3, pp. 2256-2267, Mar. 2018.

[7] S. Y. M. Mousavi, A. Jalilian, M. Savaghebi, and J. M. Guerrero. "Coordinated control of multifunctional inverters for voltage support and harmonic compensation in a grid-connected microgrid," *Electr. Power Syst. Res.*, Vol. 155, pp. 254-264, Feb. 2018.

[8] W. Wu, Y. Liu, Y. He, H. S. Chung, M. Liserre, and F. Blaabjerg. "Damping methods for resonances caused by LCL-filter-based current-controlled grid-tied power inverters: an overview," *IEEE Trans. Ind. Electron.*, Vol. 64, No. 9, pp. 7402-7413, Sep. 2017.

[9] A. Khan, A. Gastli, and L. Ben-Brahim, "Modeling and control for new LLCL filter based grid-tied PV inverters with active power decoupling and active resonance damping capabilities," *Electr. Power Syst. Res.*, Vol. 155, pp. 307-319, Feb. 2018.

[10] R. Dash, P. Paikray, and S. C. Swain, "Active power filter for harmonic mitigation in a distributed power generation system," *International Conference on Innovations in Power and Advanced Computing Technologies (i-PAGT)*, pp. 1-6, 2017.

[11] A. N. Kumar and J. I. Raglend, "Micro turbine starting and harmonic mitigation in distributed generation using active power filter," *International Conference on Innovations in Power and Advanced Computing Technologies (i-PAGT)*, pp. 1-3, 2017.

[12] G. Carpinelli, A. Russo, and P. Varilone, "Active filters: A multi-objective approach for the optimal allocation and sizing in distribution networks," *International Symposium on Power Electronics, Electrical Drives, Automation and Motion (SPEEDAM)*, pp. 1201-1207, 2014.

[13] K. Rameshkumar, V. Indragandhi, K. Palanisamy, and T. Arunkumari, "Model predictive current control of single phase shunt active power filter," *International Conference on Power Engineering, Computing and Control (PECCON)*, pp. 658-665, 2017.

[14] A. A. Valdez-Fernandez, G. Escobar, P. R. Martinez-Rodriguez, J. M. Sosa, D. U. Campos-Delgado, and M. J. Lopez-Sanchez, "Modelling and control of a hybrid power filter to compensate harmonic distortion under unbalanced operation," *IET Power Electron.*, Vol. 10, No. 7, pp. 782-791, Jun. 2017.

[15] L. Wang, C. Lam, and M. Wong, "Selective compensation of distortion, unbalanced and reactive power of a thyristor-controlled LC-coupling hybrid active power filter (TCLC-HAPF)," *IEEE Trans. Power Electron.*, Vol. 32, No. 12, pp. 9065-9077, Dec. 2017.

[16] A. Tan, K. C.Bayindir, M. U. Cuma, and M. Tümay, "Multiple harmonic elimination-based feedback controller for shunt hybrid active power filter," *IET Power Electron.*, Vol. 10, No. 8, pp. 945-956, Jun. 2017.

[17] G. Carpinelli, D. Proto, and A. Russo, "Optimal planning of active power filters in a distribution system using trade-off/risk method," *IEEE Trans. Power Del.*, Vol. 32, No. 2, pp. 841-851, Apr. 2017.

[18] M. Shivaie, A. Salemnia, and M. T. Ameli, "A multi-objective approach to optimal placement and sizing of multiple active power filters using a music-inspired algorithm," *Applied Soft Computing J.*, Vol. 22, pp. 189- 204, Sep. 2014.

[19] J. Sarker and S. K. Goswami, "Optimal location of unified power quality conditioner in distribution system for power quality improvement," *Int. J. Electr. Power Energy Syst.*, Vol. 83, pp. 309-324, Dec. 2016.

[20] A. Rosyadi, O. Penangsang, and A. Soeprijanto, "Optimal filter placement and sizing in radial distribution system using whale optimization algorithm," *International Seminar on Intelligent Technology and Its Applications (ISITIA)*, pp. 87-92, 2017.

[21] M. Mohammad, "Particle swarm optimization algorithm for simultaneous optimal placement and sizing of shunt active power conditioner (APC) and shunt capacitor in harmonic distorted distribution system," *J. Central South Univ.*, Vol. 24, No. 9, pp. 2035-2048, Sep. 2017.

[22] A. Moradifar and A. Akbari Foroud, "A hybrid fuzzy DIAICA approach for cost-effective placement and sizing of APFs," *IETE Techn. Rev.*, Vol. 34, No. 5, pp. 579-589, Sep. 2017.

[23] M. Shivaie, A. Salemnia, and M. T. Ameli, "Optimal multi-objective placement and sizing of passive and active power filters by a fuzzy-improved harmony search algorithm," *Int. Trans. Electr. Energy Syst.*, Vol. 25, No. 3, pp. 520-546, Mar. 2015.

[24] M. Maciazek, D. Grabowski, and M. Pasko, "Genetic and combinatorial algorithms for optimal sizing and placement of active power filters," *Int. J. Applied Mathematics Computer Sci.*, Vol. 25, No. 2, pp. 269-279, Jun. 2015.

[25] I. Alhamrouni, A. Khairuddin, A. F. Ferdavani, and M. Salem, "Transmission expansion planning using AC-based differential evolution algorithm," *IET Gener., Transm. & Distribut.*, Vol. 8, No. 10, pp. 1637-1644, Oct. 2014.

[26] A. M. Shaheen, R. A. El-Sehiemy, and S. M. Farrag, "Solving multi-objective optimal power flow problem via forced initialized differential evolution algorithm," *IET Gener., Transm. & Distribut.*, Vol. 10, No. 7, pp. 1634-1647, May 2016.

[27] Z. Liu, H. Wu, W. Jin, B. Xu, Y. Ji, and M. Wu, "Two-step method for identifying photovoltaic grid-connected inverter controller parameters based on the adaptive differential evolution algorithm," *IET Gener., Transm. & Distribut.*, Vol. 11, No. 17, pp. 4282-4290, Nov. 2017.

[28] J. A. P. Lopes, N. Hatziargyriou, J. Mutale, P. Djapic, and N. Jenkins, "Integrating distributed generation into electric power systems: A review of drivers, challenges and

opportunities," *Electr. Power Syst. Res.*, Vol. 77, No. 9, pp. 1189-1203, Jul. 2007.

[29] K. Yamashita, S. Djokic, J. Matevosyan, F. O. Resende, L. M. Korunovic, Z. Y. Dong, and J. V. Milanovic, "Modelling and aggregation of loads in flexible power networks c scope and status of the work of CIGRE WG C4.605," *8th Power Plant and Power System Control Symposium (PPPSC)*, pp. 405-410, 2012.

[30] E. O. Kontis, T. A. Papadopoulos, G. A. Barzegkar-Ntovom, A. I. Chrysochos, and G. K. Papagiannis, "Modal analysis of active distribution networks using system identification techniques," *Int. J. Electr. Power & Energy Syst.*, Vol. 100, pp. 365-378, Sep. 2018.

[31] J. Teng, "Modelling distributed generations in three-phase distribution load flow," *IET Gener., Transm. & Distribut.*, Vol. 2, No. 3, pp. 330-340, May 2008.

[32] J. Teng, S. Liao, and R. Leou, "Three-phase harmonic analysis method for unbalanced distribution systems," *Energies*, Vol. 7, No. 1, pp. 365- 384, Jan. 2014.

Yougen Chen was born in China, in 1976. He received his B.S. degree in Electrical Engineering from the Changsha Railway University, Changsha, China, in 1998; his M.S. degree in Traffic Information Engineering Control from Central South University, Changsha, China, in 2003; and his Ph.D. degree in Intelligent Control from the University of Tsukuba, Tsukuba, Japan, in 2009. He was with the CRRC Zhuzhou Institute Co., Ltd., Zhuzhou, China, where he worked on the development of photovoltaic power generation applications, from 2010 to 2013. He is presently working as an Assistant Professor in the School of Automation, Central South University. His current research interests include electric power system planning, multiple criteria decision-making, and power electronics and control in distributed generation fields.

Weiwei Chen was born in China, in 1993. He received his B.S. degree in Measurement Control Technology and Instruments from Central South University, Changsha, China, in 2016; and his M.S. degree in Electrical Engineering from Central South University, Changsha, China, in 2019. He is presently working as an Assistant Engineer in the Energy Planning and Research Center, China Energy Engineering Group Guangxi Electric Power Design Institute Co., Ltd., Nanning, China. His current research interests include power system planning and optimal dispatch, energy storage systems, multiple attribute decision-making methods and their application in power systems.

Renli Yang was born in China, in 1987. He received his B.S. degree in Automation from Shenzhen University, Shenzhen, China, in 2011; and his M.S. degree in Electrical Engineering from Central South University, Changsha, China, in 2014. In 2014, he joined the Maoming Power Supply Bureau of the Guangdong Power Grid Co., Ltd., Xinyi, China. He is presently the Deputy Group Leader of the Distribution Dispatching Automation Group of the Maoming Power Supply Bureau. His current research interests include grid connection of distributed new energy, and distribution automation control.

Zhiyong Li was born in China, in 1972. He received his B.S. degree in Radio Technology from the Nanjing University of Science and Technology, Nanjing, China, in 1994; his M.S. degree in Traffic Information Engineering and Control from Changsha Railway University, Changsha, China, in 2000; and his Ph.D. degree in Control Theory and Control Engineering from Central South University, Changsha, China, in 2006. Since 2007, he has been working at Central South University, where he is presently an Associate Professor in the School of Automation. His current research interests include power quality, microgrid technology, photovoltaic power generation and its application.